Renewable and Sustainable Energy Reviews 31 (2014) 501–508

Contents lists available at ScienceDirect

Renewable and Sustainable Energy Reviews

journal homepage: www.elsevier.com/locate/rser

Interfacing renewable energy sources for maximum power transfer—Part I: Statics

Shlomo Gadelovits [a], Alon Kuperman [a,*], Moshe Sitbon [a], Ilan Aharon [a,b], Sigmond Singer [b]

[a] Hybrid Energy Sources Laboratory, Dept. of Electrical Engineering and Electronics, Ariel University, POB 3, Ariel 40700, Israel
[b] School of Electrical Engineering, Dept. of Systems Electrical Engineering, Tel-Aviv University, POB 39040, Tel-Aviv 6997801, Israel

ARTICLE INFO

Article history:
Received 9 April 2013
Received in revised form
18 December 2013
Accepted 19 December 2013
Available online 20 January 2014

Keywords:
Renewable energy
Power processing
Maximum power line

ABSTRACT

The manuscript presents a method of interfacing renewable energy generators by means of Maximum Power Line tracking rather than Maximum Power Point tracking. The maximum power line connects the maximum power points of output *I–V* curves of a source for different values of power producing parameter (wind, solar insolation etc.) and may be estimated offline with moderate accuracy. As a result, during the online operation, the maximum power point tracker only has to compensate for maximum power line inaccuracy and changes caused by slow temperature variations and system parameters drift. The approach allows reducing dramatically the bandwidth of the MPP tracking algorithms and simplifying the implementation, making analog MPP trackers a viable choice. The proposed method is shown to be a generalized version of the well-known loss-free resistor concept, referred to as loss-free load in the manuscript. Several particular case examples of the proposed method presented in the literature are reviewed.

Contents

1. Introduction

Global economy prompt development has led to remarkable increase in energy requirements both in emergent [1] and well established countries [2]. The lessening of fossil fuels resources along with excessive carbon emissions has increased interest in both energy saving and increased adoption of renewable energy sources [3,4], including biomass, hydropower, geothermal, solar, wind and marine energies. Today, the renewable energy sources share of the total world energy production is around 14% and expected to increase significantly until the end of the century [5].

Photovoltaic (PV) and wind powers are probably the strongest-growing electricity generating technologies, demonstrating recent annual growth rates of around 40% and 34%, respectively [6]. PV technology is one of the best ways to harvest the solar energy, since PV devices are strong and simple in design, requiring very little maintenance and capable of giving outputs from microwatts to megawatts. This is why they are used as power sources in water pumping, remote buildings, solar home systems, communications, satellites and space vehicles, reverse osmosis plants, and even megawatt-scale power plants [7,8]. Wind energy represents a relevant electricity production technology in some European

* Corresponding author. Tel.: +972 526943234; fax: +972 3 9066238.
E-mail address: alonku@ariel.ac.il (A. Kuperman).

1364-0321/$ - see front matter © 2014 Elsevier Ltd. All rights reserved.
http://dx.doi.org/10.1016/j.rser.2013.12.039

countries and is called to play a crucial role in the future energy supply worldwide [9]. Power generation through wind has an advantage over other applications of renewable energy technologies based on its technological maturity, good infrastructure and relative cost competitiveness [10]. This work focuses on these two technologies but can be easily extended to the other renewable energy sources as well.

Efficiency still remains the main weakness of both PV and wind energy technologies. Modern solar cells are struggling to reach the theoretical thermodynamic efficiency limits (40.6% and 63.6% for single and triple junction cells, respectively) and wind turbines output is well below 59.3% Betz limit. As a result, further conversion losses must be minimized in order to increase the feasibility of renewable energy production. Moreover, the rated power of the installed system must be well matched to the operating site in order to achieve the best trade-off between the capacity (utilization) factor and annual energy yield thus minimizing the return of investment time [11,12].

Nevertheless, the importance of both source efficiency and amount of energy captured is marginal if the renewable energy generator is incorrectly matched to the load. The output of the most efficient cell under very rich illumination can still yield low power output if the electrical operating point is improper. The same is valid for an improperly loaded wind turbine operating in a high wind speed region. As a matter of fact, the electrical characteristics of a solar panel and the mechanical characteristics of a wind turbine possess single maximum power point (MPP) for given ambient conditions. Such a behavior (frequently referred to as soft source characteristics) is common to any renewable energy source. Thus, correct sizing and matching to the load in order to extract maximum possible power is of an extreme significance.

The commonly used matching method is based on inserting a power converter between the renewable energy generator (REG) and the load in order to force the operating point follow the MPP upon the environmental conditions variation. MPP tracking algorithms have evolved over the last two decades along with the tremendous increase of the computational power and power semiconductor technology progress and exist for both PV [13] and wind [14] energy generation. REG output is usually dependent on both the load and environmental operating conditions. Moreover, a single environmental parameter may be referred to as power producing (solar irradiation for PV panels, wind for wind turbines), while the others only influence power output without directly causing it. The most prominent parameter is temperature, having a great effect on the power productivity of both PV and wind REGs. It is important to note that the power producing parameter variations are usually relatively fast compared to the temperature rate of change. The MPP tracker must be able to follow the maximum energy production point which varies with any environmental operating condition change. As a result, its bandwidth is usually higher than the solar irradiation or the wind speed spectrum rates of change, requiring relatively high computational power and suffering from high frequency noise and even instability in some extreme cases.

The manuscript goal is to present a method of interfacing REGs by means of a Maximum power line (MPL) rather than MPP in steady state (statics). The MPL connects the loci of all MPPs caused by the power producing parameter variations and may be estimated offline with moderate accuracy. As a result, during online operation the MPP tracker only has to compensate for MPL inaccuracy and changes caused by slow temperature variations. This allows reducing dramatically the bandwidth of the MPP tracking algorithms and simplifying the implementation, making analog MPP trackers a viable choice.

The rest of the manuscript is arranged as follows. Section 2 reveals the characteristics of a general soft source. Loss-free resistor based Maximum power point tracking is revised in Section 3 and the concept generalization is derived in Section 4. The application of generalized LFR based MPP tracking to wind turbine and PV REGs is demonstrated in Sections 5 and 6, respectively. A short discussion in Section 7 is followed by the manuscript conclusions in Section 8.

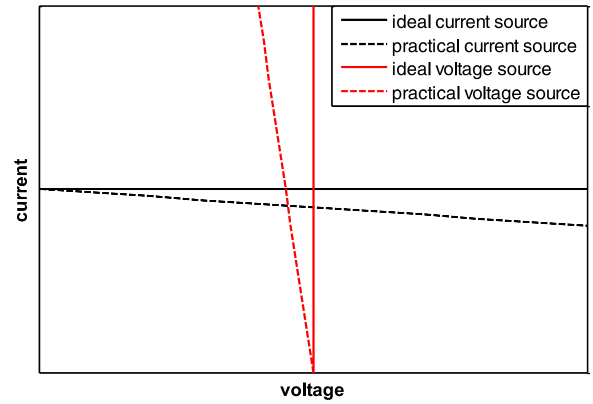


Fig. 1. *I–V* characteristics of ideal and practical rigid DC sources.

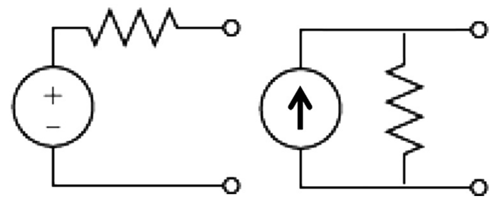


Fig. 2. Rigid Thevenin voltage (left) and Norton current (right) sources equivalent circuits.

2. Soft source versus rigid source

Ideal voltage/current source is defined as device capable of supplying rated voltage/current at any load, possessing linear *I–V* characteristics with infinite/zero slope, as shown in Fig. 1.

In practice, ideal voltage/current sources do not exist. Instead, rigid sources are commonly used. DC rigid sources possess non-zero internal resistance and may be represented by Thevenin/Norton equivalent circuits, as shown in Fig. 2. These sources supply near rated voltage/current from zero to nominal load, possessing linear *I–V* characteristics with a slope, as shown in Fig. 1.

Since such sources are designed to be as close to ideal as possible, the internal resistance of a DC rigid voltage source is as small as possible and in the case of a DC rigid current source the internal resistance is as high as possible [15]. Obviously, such sources are influenced by the load; however, the voltage/current drop at the heaviest load (and hence at any lighter load) is negligible compared to the rated voltage/current supplied by the source.

On the contrary, soft sources possess nonlinear *I–V* characteristics and cannot be unambiguously defined as voltage or current sources (rather, it is often referred to as power source). Moreover, the voltage is heavily influenced by the load, usually possessing a maximum value at no-load conditions and minimum value (possibly zero) at maximum loading. A typical soft source *I–V* curve is shown in Fig. 3. Note that since the power is zero at both open circuit and short circuit conditions, a MPP (typically unique for a single source) exists, defined by $p_M = v_M \times i_M$, i.e. the maximum power will be delivered by the soft source only at the unique operation point (v_M, i_M). All renewable energy sources possess soft

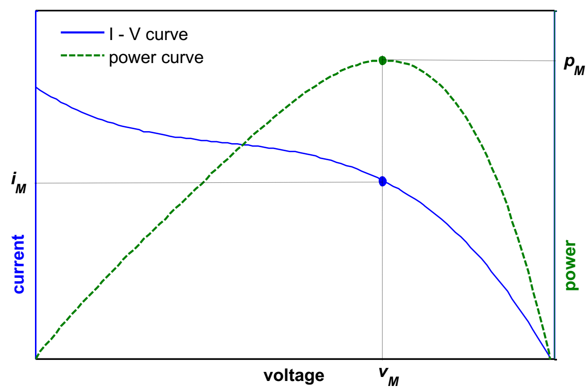


Fig. 3. *I–V* and *P–V* characteristics of a soft source.

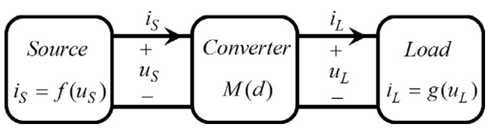


Fig. 4. Source–load interfacing by means of a DC–DC converter.

source characteristics. In addition, the *I–V* curve and therefore the MPP change with environmental conditions variations. Hence, an MPP tracker main goal is forcing the soft source "see" a load whose *I–V* characteristics intersects its own *I–V* curve at MPP for any environmental conditions.

3. Interfacing soft source for maximum power transfer

Consider a soft source, characterized by the following *I–V* and *P–V* curves for given environmental conditions,

$$i_S = f(u_S) \tag{1}$$

and

$$p_S = u_S i_S = u_S f(u_S), \tag{2}$$

respectively, connected to an arbitrary load with subsequent *I–V* characteristics

$$i_L = g(u_L), \tag{3}$$

via a power processing unit (e.g. DC–DC converter) with duty cycle (d) dependent static voltage ratio

$$\frac{u_L}{u_S} = M(d), \tag{4}$$

as shown in Fig. 4.

The source and load powers are related via

$$u_L i_L = p_L = \eta p_S = \eta u_S i_S, \tag{5}$$

where η is the converter efficiency. Hence, the *I–V* curve of the load "seen" by the soft source may be expressed as

$$i_S = \frac{M(d) \times i_L}{\eta} = \frac{M(d) \times g(u_L)}{\eta} = \frac{M(d) \times g(M(d) \times u_S)}{\eta} = h(d, u_S) \tag{6}$$

The MPP current, voltage and duty cycle are then linked as

$$i_M = g(u_M) = h(d_M, u_M) = \frac{M(d_M) \times g(M(d_M) \times u_M)}{\eta} \tag{7}$$

In a particular case of general linear load, shown in Fig. 5 with an *I–V* curve given by

$$u_L = u_0 + i_L r_0, \tag{8}$$

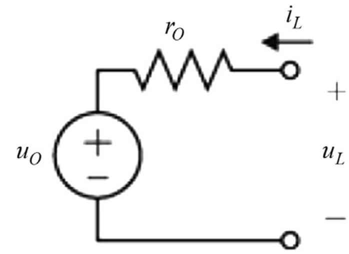


Fig. 5. General linear load.

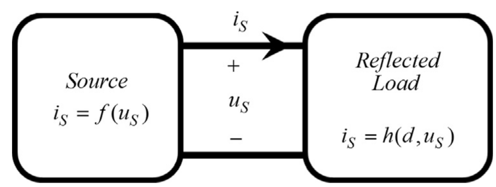


Fig. 6. Load as "seen" by the soft source.

Eq. (7) may be simplified as

$$i_M = M(d_M) \times \frac{M(d_M) \times u_M - u_0}{\eta r_0} \tag{9}$$

Further rearranging (9) leads to

$$M^2(d_M) - M(d_M) \times \frac{u_0}{u_M} - \eta \times r_0 \times \frac{i_M}{u_M} = 0, \tag{10}$$

Yielding a feasible solution for the static voltage ratio given by

$$M(d_M) = \frac{u_0}{2u_M} + \sqrt{\left(\frac{u_0}{2u_M}\right)^2 + \eta r_0 \frac{i_M}{u_M}} \tag{11}$$

The power processing unit actually performs a transformation of the load *I–V* curve defined by (3) into a reflected load given by (6), as shown in Fig. 6 [16]. If the converter duty cycle is set according to (11), the source and reflected load characteristics intersect at MPP as demonstrated in Fig. 7.

It is worth noting that any intersection between $f(u_S)$ and $h(d, u_S)$ explicitly defines the amount of power (2), supplied by the soft source to the power processing unit and transferred to the load. Hence from the load point of view, it is supplied by a power source rather than voltage or current source, as shown in Fig. 8.

Power source is an element whose *I–V* characteristics obeys the following equation, $vi = p, |v| < \infty, |i| < \infty$ for $p > 0$ [17]. The symbol of power source and its *I–V* characteristics in case p is constant (such load is referred to as constant power source) are shown in Fig. 9.

The most important property of such a source is negative dynamic impedance, i.e. the raise of current leads to voltage decrease and vice–versa. Moreover, short and open circuiting of such an element are non-feasible. The resulting load side source and load characteristics are demonstrated in Fig. 10, describing the effect of constant power source.

In case of a nonlinear load or of a linear load with unknown characteristics, it is not easy if at all possible to obtain the optimal static voltage ratio from (7). In such a case loss-free resistor (LFR) approach [18] is often employed. Instead of attempting to reflect the load *I–V* curve, the load "seen" by the soft source is emulated as a controlled resistor, i.e.

$$i_S = \frac{u_S}{r_S(d)} \tag{12}$$

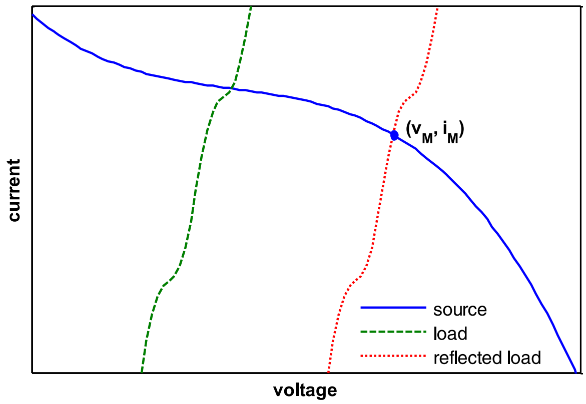


Fig. 7. *I–V* characteristics of the soft source, load and power processed (reflected) load.

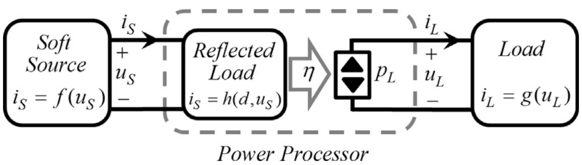


Fig. 8. Power processing chain of a soft source interfacing.

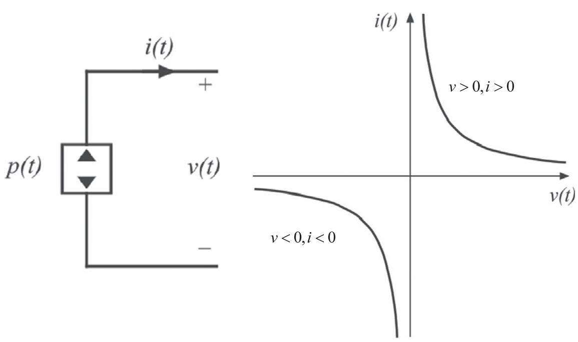


Fig. 9. Power source symbol (left) and *I–V* curve (right).

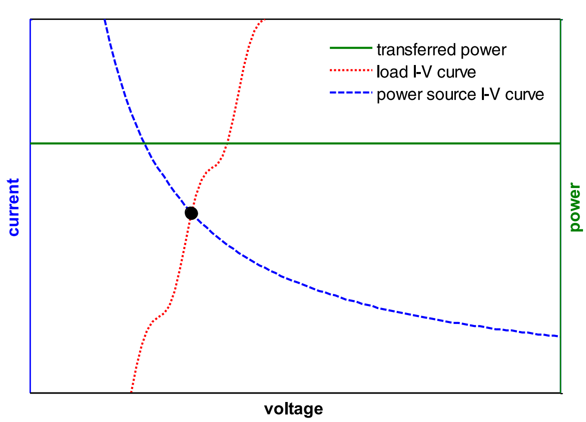


Fig. 10. Effect of constant power source—power is independent on operating point.

The source operating point is then determined by

$$f(u_S) = \frac{u_S}{r_S(d)} \tag{13}$$

and the power drawn from the source is obtained as

$$p_S = f^2(u_S) \times r_S(d) = \frac{u_S^2}{r_S(d)} \tag{14}$$

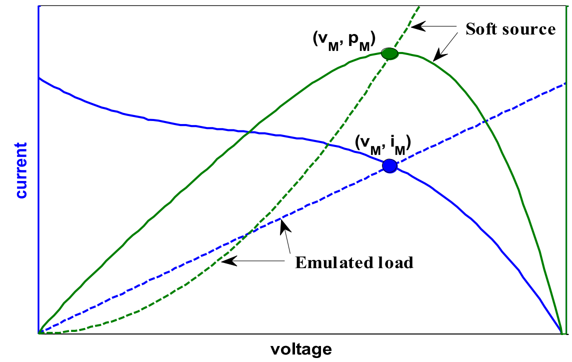


Fig. 11. LFR-based MPP tracking.

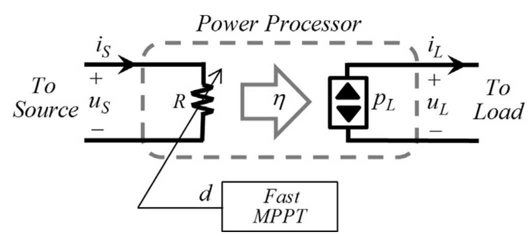


Fig. 12. Adjusting the LFR by a fast MPP tracking algorithm.

At the MPP, the emulated resistance satisfies

$$r_S(d_M) = \frac{u_M}{f(u_M)} = \frac{u_M}{i_M}, \tag{15}$$

as shown in Fig. 11.

In case of a general linear load, combining (14) with (5) and (8) leads to

$$u_L^2 - u_L \times u_0 - f^2(u_S) \times r_S(d) \times r_0 \times \eta = 0, \tag{16}$$

solution of which yields the following load operating point

$$\begin{aligned} u_L &= \frac{u_0}{2} + \sqrt{\left(\frac{u_0}{2}\right)^2 + f^2(u_S) \times r_S(d) \times r_0 \times \eta} \\ &= \frac{u_0}{2} + \sqrt{\left(\frac{u_0}{2}\right)^2 + \frac{u_S^2}{r_S(d)} \times r_0 \times \eta} \end{aligned} \tag{17}$$

Since the environmental conditions are seldom constant, an MPP tracker constantly varies the emulated resistance by changing the duty cycle appropriately, as shown in Fig. 12 [19,20].

4. Generalizing the LFR-based MPP tracking concept

It was shown in the literature that in both PV and wind turbine based REGs any environmental condition variation necessitates a change of the LFR value [18–20]. Hence, in order to track the optimum operation point changes as accurate as possible, the LFR-based MPP tracking bandwidth should exceed the speed of environmental parameters rate of change. Such an operation requires relatively high computational power, suffers from high frequency noise and even stability loss. As mentioned in the introduction, the power producing environmental parameter possesses the fastest variations, while temperature changes are relatively slow. If the MMP tracking algorithm was insensitive to the fast variations of the power producing environmental parameter, all the above mentioned problems would become much less severe. In addition, less computational power would be needed, simplifying the MMP tracking digital hardware and making analog implementation more feasible. Generalizing the LFR-based MMP tracking concept, allowing reducing the

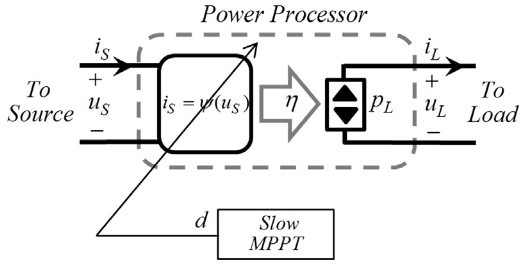


Fig. 13. Adjusting the LFL by a slow MPP tracking algorithm.

sensitivity of MPP algorithm to power producing parameter variations, is presented next.

Recall that (1) is valid for some specific environmental conditions. As stated above, in general case the *I–V* curve depends on several environmental parameters, two of which (the power producing parameter ξ and temperature *T*) are the most prominent. For any given ξ and *T*, unique MPP relation exists according to

$$i_M = f(u_M, \xi, T) \tag{18}$$

Consider a time period where the temperature is nearly constant. During this period, the MPP depends on the power producing parameter only. Therefore, an explicit *I–V* curve exists,

$$i_S = \psi(u_S), \tag{19}$$

Connecting the MPPs for all possible values of ξ [21]. In general, ψ is temperature-dependent function, but its variations are relatively slow as mentioned. Hence, if the power processing unit is able to emulate a load according to (19) during the above mentioned time period as shown in Fig. 13, the soft source would operate at MPP for any value of the power producing parameter ξ.

The approach may be defined as Maximum Power Line (MPL) tracking rather than MPP tracking. Here, the power processor actually emulates a loss free load (LFL), which is a generalized version of the LFR. Moreover, as will be shown in the next subsections slow environmental condition (temperature) variations only necessitate LFL value changes as opposed to LFR-based MPP tracking. Hence some tracking mechanism would still be beneficial; however its role comes down to adjusting ψ according to temperature variations, which is a very low bandwidth control function.

5. Application to wind turbine REG

Consider a wind turbine based REG, interfaced by a DC–DC converter as power processor. Two arrangements are possible, depending on the machine type, as shown in Fig. 14. In general, the wind turbine is connected to an electrical through mechanical transmission (G). In case a DC generator (DCG) is employed, its output is connected directly to the power processor. If the REG is based on an AC generator (ACG), its output is first rectified by a diode bridge and then fed into the power processor. Note that the presented method may be easily extended to the case where ACG is interfaced by an active AC–DC converter; however this arrangement is not discussed for the sake of brevity.

Note that the theory in the preceding sections was presented for electrical sources. The wind turbine REG may be represented as DC electrical source with output characteristics based on (i_G, v_G), as shown in Fig. 14. The derivation of these characteristics is shown next for the Permanent Magnet (PM) DCG case only (without loss of generality) because of relative simplicity. Nevertheless, the results are similar to the PM ACG case, see [22–25] for details.

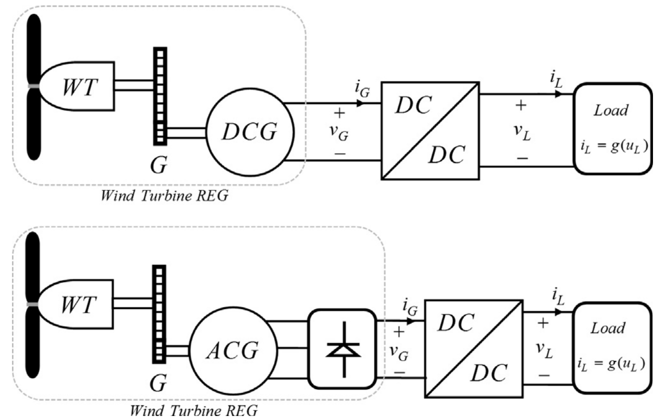


Fig. 14. Interfacing a DC (upper) and AC (lower) generator based wind turbine REG.

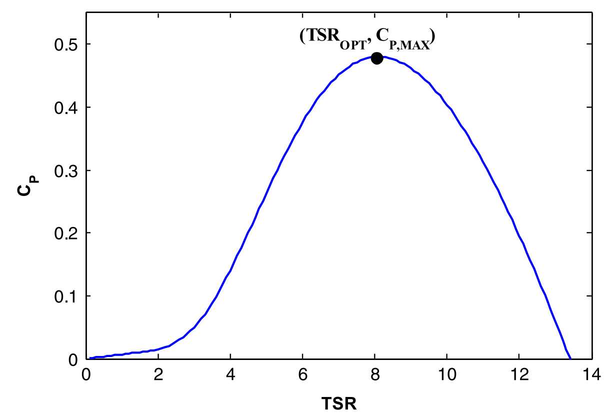


Fig. 15. Typical power coefficient versus tip–speed ratio curve.

The mechanical power extracted from wind by a wind turbine is given by

$$P_T = \frac{1}{2}\rho A C_P v_W^3, \tag{20}$$

where ρ is air density (temperature dependent), *A* is the area swept by the turbine's blades, v_W is wind speed and C_P is power coefficient which is a nonlinear function of blades pitch angle β and turbine tip–speed ratio (*TSR*),

$$TSR = \frac{\omega_T R}{v_W} \tag{21}$$

with ω_T —turbine rotational speed and *R*—blade radius. Eq. (20) can be then rewritten as

$$P_T = \frac{1}{2}\rho A C_P \left(\frac{R}{TSR}\right)^3 \omega_T^3 \tag{22}$$

Typical $C_P(TSR)$ curve for $\beta = 0$ is presented in Fig. 15, possessing a single MPP as shown.

Note that (TSR_{OPT}, $C_{P,MAX}$) pair is constant for a given wind turbine design. As a result, for a given wind speed maximum power is extracted from the wind if the turbine rotates at the following rotational speed,

$$\omega_{T,OPT} = \frac{TSR_{OPT}}{R} v_W \tag{23}$$

The maximum power is obtained by combining (23) and (20) as

$$P_{T,MAX} = \frac{1}{2}\rho A C_{P,MAX} \left(\frac{R}{TSR_{OPT}}\right)^3 \omega_{T,OPT}^3 = K_{OPT}\omega_{T,OPT}^3 \tag{24}$$

with constant K_{OPT}. Hence, a curve given by

$$P_{T,OPT}=K_{OPT}\omega_T^3 \tag{25}$$

Connects all the MPPs of turbine power curves, as shown in Fig. 16.

Moreover, the curve connecting all the optimal turbine torque points, leading to maximum power extraction may be expressed as

$$T_T=\frac{P_{OPT}}{\omega_T}=K_{OPT}\omega_T^2, \tag{26}$$

Defining the mechanical MPL of the wind turbine. The next step is reflecting (26) to the electrical output of the REG in order to derive the electrical MPL to be emulated by power processor.

The mechanical transmission relates turbine and generator speeds and torques as

$$n=\frac{\omega_G}{\omega_T}=\frac{\eta_{GEAR}T_T}{T_G}, \tag{27}$$

where ω_G and T_G are generator rotational speed and torque, respectively and n and η_{GEAR} are transmission gear ratio and efficiency, respectively. The wind turbine mechanical MPL (26) may be then referred to the generator side as

$$T_G=\eta_{GEAR}K_{OPT}\frac{\omega_G^2}{n^3} \tag{28}$$

The torque–speed characteristics of a DC machine (neglecting air gap and iron losses) is given by

$$\omega_G=\frac{u_G}{K_T}-\frac{R}{K_T^2}T_G, \tag{29}$$

where R is armature resistance, K_T is torque constant and the steady state generator torque is related to the armature current as

$$T_G=K_T i_G \tag{30}$$

Combining (28)–(30), the electrical MPL of a wind turbine REG is obtained as

$$Ri_G+\sqrt{\frac{n^3K_T^3}{\eta_{GEAR}K_{OPT}}i_G}=u_G \tag{31}$$

Comparing to (19), the MPL is given in an inverse form, $u_G=\psi^{-1}(i_G)$; however the meaning is the same: if the power processor is able to emulate the derived LFL, i.e. to adjust the REG voltage according to (31), the wind turbine would operate at MPP for any wind speed. It is worth noting that ψ^{-1} depends on K_{OPT}, which in turn is a function of the temperature dependent air density. Hence the power processor should include some closed-loop tracking mechanism, which would slowly adjust u_G, employing (31) as feed-forward term. This would be beneficial as well for compensating slowly varying system uncertainties and disturbances occurring as a result of e.g. ageing, frequent mechanical stresses etc.

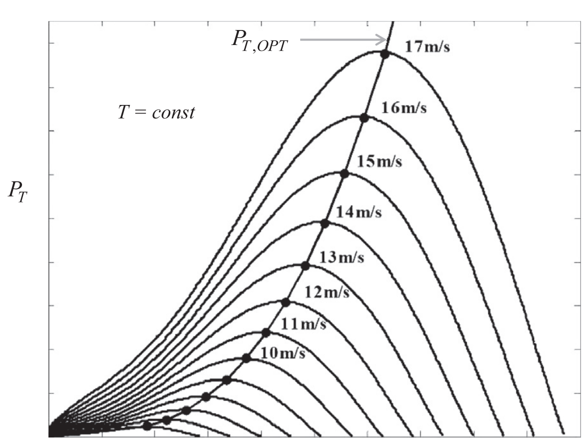


Fig. 16. Speed–power curves of a wind turbine.

6. Application to photovoltaic REG

Consider a PV based REG, interfaced by a DC–DC converter as power processor (without loss of generality), as shown in Fig. 17.

A PV cell/panel output characteristics are typically described by a family of monotonic, nonlinear *I–V* curves, as shown in Fig. 18. The single-exponential approximation of PV REG output characteristics provides a good trade-off between the simplicity and accuracy and is given by [26]

$$i_G=I_{PV}-I_0\left[\exp\left(\frac{u_G+R_Si_G}{V_Ta}\right)-1\right]-\frac{u_G+R_Si_G}{R_P}, \tag{32}$$

where I_{PV} and I_0 are insolation dependent photovoltaic and temperature dependent saturation currents, respectively, V_T is temperature dependent thermal voltage, a is the ideality constant and R_S and R_P are the equivalent series and parallel resistances, respectively.

Note that since (32) describes a monotonically decreasing function, each *I–V* curve possesses a single MPP marked with a circle in Fig. 18. Hence, an MPL connecting all the MPPs may be obtained employing nonlinear resistive maximum power theorem [21] as [27]

$$\frac{u_G}{i_G}=R_S+\left[\frac{I_0}{V_Ta}\exp\left(\frac{u_G+R_Si_G}{V_Ta}\right)+\frac{1}{R_P}\right]^{-1} \tag{33}$$

Comparing to (19), the MPL is given in an implicit form and may be expressed either in direct direct $i_G=\psi(u_G,i_G)$ or inverse $u_G=\psi^{-1}(u_G,i_G)$ form. It is shown graphically in Fig. 18. If the power processor is able to emulate the derived LFL, i.e. to adjust the REG voltage according to (33), the PV panel would operate at MPP for any insolation level. It is worth noting that ψ is governed by I_0 and V_T, which are temperature dependent, hence the power processor should include some closed-loop tracking mechanism as well, which would slowly adjust u_G or i_G, employing (33) as feed-forward term. In addition, this would be useful for compensating

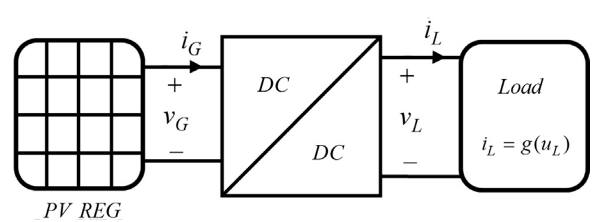


Fig. 17. Interfacing a PV REG.

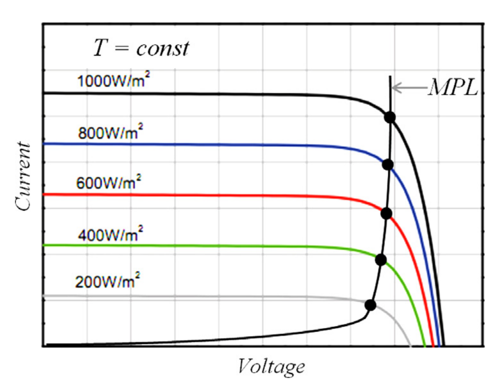


Fig. 18. *I–V* curves of a PV REG.

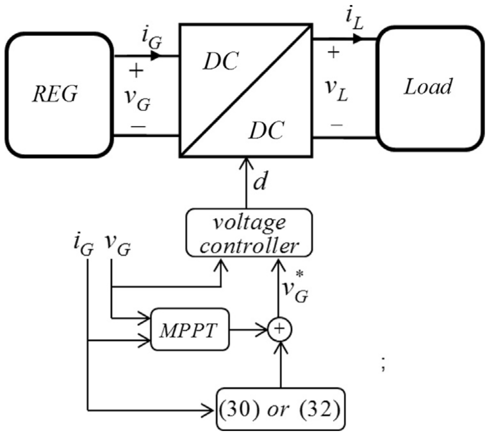


Fig. 19. System structure of interfacing an REG.

slowly varying system uncertainties and disturbances occurring as a result of e.g. dust, PV panel ageing etc.

7. Discussion

Derivation of MPL expressions for both wind turbine and PV REGs have revealed that explicit LFL exist in both cases for constant temperatures. Moreover, since the expressions given by (31) and (33) depend on system parameters as well as on temperature, their open loop employment may result in suboptimal performance because of daily and seasonal temperature variations and unavoidable long time system parameter changes. Therefore an external MPP tracking loop should be added to load emulating algorithm in order to assure accurate short and long term performance. The suggested overall system structure is shown in Fig. 19. The power processor is controlled be duty cycle d, created by an input voltage controller. The reference REG voltage v_G^* is formed by two terms: the feedforward term, given by (31) or (33) and adjusting term, created by a slow MPP tracking controller. Note that voltage controller may be replaced by a current controller, thus the feedforward and adjusting terms would be currents rather than voltages.

Since an MPP tracking driven adjusting voltage term exists, (31) and (33) may not be followed exactly. In [28] the lower arrangement of Fig. 14 was presented and armature impedance of the ACG was neglected, i.e. the first term of (31) was absent leading to the MPL of the following simplified form,

$$i_G = K u_G^2 \tag{34}$$

A current controller was implemented to control the REG output current while Perturb-and-Observe MPP tracking algorithm was employed to adjust the parameter K. In [29], the authors point out that the MPL of a PV REG may be relatively accurately approximated by a straight line for insolation levels above 300 W m^{-2}. Therefore instead of implementing an implicit function given by (33), linear explicit relation given by

$$v_G = a + b i_G \tag{35}$$

with MPPT-adjusted a and b may be implemented, leading to accelerated convergence. Extending this approach, the authors of [30] revealed that the MPL of a PV REG may be further approximated by a straight vertical line for insolation levels above 500 W m^{-2}. The MPL was approximated for an average seasonal temperature of Southern Israel and no MPP tracking based adjustment was maid. Considering ten-year measured meteorological data, presented system extracted only 1.1% less energy compared to a simulated yield of system with an ideal MPP tracking mechanism. Note that the two latter applications may be partly of fully implemented using analog controllers only, increasing the system reliability and decreasing the cost.

8. Conclusions

In this paper, a Maximum Power Line tracking based method of interfacing renewable energy generators was presented, opposed to the commonly acceptable Maximum Power Point tracking algorithms. The maximum power line is the maximum power loci for possible power producing parameter (wind, solar insolation etc.) values and may be estimated offline without imposing high accuracy requirement. Therefore during the real time operation, the maximum power point tracker only has to compensate for maximum power line inaccuracy and changes caused by slow temperature variations and system parameters drift due to aging and harsh operating conditions. The approach makes possible to significantly reduce the speed of the MPP tracking algorithms and simplify the implementation, making analog MPP trackers a practicable choice. The proposed method was also shown to be a generalized version of the well-known loss-free resistor concept and is referred to as loss-free load in the manuscript. Several particular case examples of the proposed method presented in the literature were reviewed, enforcing the proposed method.

References

[1] El Fadel M, Rachid G, El-Samra R, Bou Boutros G, Hashisho J. Knowledge management mapping and gap analysis in renewable energy: towards a sustainable framework in developing countries. Renewable Sustainable Energy Rev 2013;20:576–84.
[2] Marques A, Fuinhas J. Drivers promoting renewable energy: a dynamic panel approach. Renewable Sustainable Energy Rev 2011;15:1601–8.
[3] Banos R, Manzano-Agugliaro F, Montoya F, Gil C, Alcayde A, Gomez J. Optimization methods applied to renewable and sustainable energy: a review. Renewable Sustainable Energy Rev 2011;15:1753–66.
[4] Panwar N, Kaushik S, Kothari S. Role of renewable energy sources in environmental protection: a review. Renewable Sustainable Energy Rev 2011;15:1513–24.
[5] Manzano-Agugliaro F, Alcayde A, Montoya F, Zapata-Sierra A, Gil C. Scientific production of renewable energies worldwide: an overview. Renewable Sustainable Energy Rev 2013;18:134–43.
[6] Lenzen M. Current state of development of electricity-generating technologies: a literature review. Energies 2010;3:462–591.
[7] Parida B, Iniyan S, Goic R. A review of solar photovoltaic technologies. Renewable Sustainable Energy Rev 2011;15:1625–36.
[8] Razykov T, Ferekides C, Morel D, Stefanakos E, Ullal H, Upadhyaya H. Solar photovoltaic electricity: current status and future prospects. Sol Energy 2011;85:1580–608.
[9] Schallenberg-Rodriguez J. A methodological review to estimate techno-economical wind energy production. Renewable Sustainable Energy Rev 2013;21:272–87.
[10] Herbert G, Iniyan S, Sreevalsan E, Rajapandian S. A review of wind energy technologies. Renewable Sustainable Energy Rev 2007;11:1117–45.
[11] Leijon M, Skoglund A, Waters R, Rehn A, Lindahl M. On the physics of power, energy and economics of renewable electric energy sources—Part I. Renewable Energy 2010;35:1729–34.
[12] Skoglund A, Leijon M, Rehn A, Lindahl M, Waters R. On the physics of power, energy and economics of renewable electric energy sources—Part II. Renewable Energy 2010;35:1735–40.
[13] Abdullah M, Yatim A, Tan C, Saidur R. A review of maximum power point tracking algorithms for wind energy systems. Renewable Sustainable Energy Rev 2012;16:3220–7.
[14] Reisi A, Moradi M, Jamasb S. Classification and comparison of maximum power point tracking techniques for photovoltaic system: a review. Renewable Sustainable Energy Rev 2013;19 (433–443).
[15] Beck Y, Nehab L, Singer S. On compatibility of capacitive based converters to soft sources. In: Proceedings of IEEE 26th convention of electrical and electronic engineering in Israel; 2010; 124–128.
[16] Singer S, Braunstein A. Maximum power transfer from a nonlinear energy source to an arbitrary load. IEE Proc 1987;134:281–7.
[17] Singer S, Erickson R. Power-source element and its properties. IEE Proc Circ Dev Syst 1994;141:220–6.
[18] Valderrama-Blavi Alonso C, Martinez-Salamero L, Singer S, Estibals B, Maixe-Altes J. AC-LFR concept applied to modular photovoltaic power conversion chains. IEEE Proc Electr Power Appl 2002;149:441–8.
[19] Lee J, Bae H, Cho B. Resistive control for a photovoltaic battery charging system using a microcontroller. IEEE Trans Ind Electron 2008;55:2767–75.

[20] Tan Y, Panda S. Optimized wind energy harvesting system using resistance umulator and active rectifier for wireless sensor nodes. IEEE Trans Power Electron 2011;26:38–50.
[21] Wyatt J, Chua L. Nonlinear resistive maximum power theorem, with solar cell application. IEEE Trans Circ Syst 1983;30:824–8.
[22] Tan K, Islam S. Optimum control strategies in energy conversion of PMSG wind turbine system without mechanical sensors. IEEE Trans Energy Convers 2004;19:392–9.
[23] Chen Z, Spooner E. Grid power quality with variable speed wind turbines. IEEE Trans Energy Convers 2001:148–54.
[24] Adam M, Xavier R, Frdric R. Architecture complexity and energy efficiency of small wind turbines. IEEE Trans Ind Electron 2007;54:660–70.
[25] Zhang H, Fletcher J, Greeves N, Finney S, Williams B. One-power-point operation for variable speed wind/tidal stream turbines with synchronous generators. IET Renew Power Gener 2011;5:99–108.
[26] Villalva M, Gazoli J, Filho E. Comprehensive approach to modeling and simulation of photovoltaic arrays. IEEE Trans Power Electron 2009;24: 1198–208.
[27] Batushansky Z, Kuperman A. Thevenin based approach to PV arrays maximum power prediction. In: Proceedings of IEEE 26th convention of electrical and electronic engineering in Israel; 2010; 598–602.
[28] Xia Y, Ahmed K, Williams B. Wind turbine power coefficient analysis of a new maximum power point tracking technique. IEEE Trans Ind Electron 2013;60:1122–32.
[29] Sokolov M, Shmilovitz D. A modified MPPT scheme for accelerated convergence. IEEE Trans Energy Convers 2008;23:1105–7.
[30] Kuperman A, Averbukh M, Lineykin S. Maximum power point matching versus maximum power point tracking for solar generators. Renewable Sustainable Energy Rev 2013;19:11–7.